

Melt Diffusion-Moderated Crystal Growth and its Effect on Euhedral Crystal Shapes

Martin F. Mangler ^{1,*}, Madeleine C.S. Humphreys¹, Eshbal Geifman^{1,2}, Alexander A. Iveson ¹, Fabian B. Wadsworth¹,
Richard A. Brooker³, Amanda Lindoo^{1,3} and Keiji Hammond⁴

¹Department of Earth Sciences, Durham University, Durham DH1 3LE, UK

²Department of Geology, Trinity College Dublin, Durham D02 F227, Ireland

³School of Earth Sciences, University of Bristol, Bristol BS8 1RJ, UK

⁴American Museum of Natural History, New York NY 10024, USA

*Corresponding author. E-mail: martin.mangler@durham.ac.uk

Abstract

Crystal growth is often described as either interface-controlled or diffusion-controlled. Here, we study crystal growth in an intermediate scenario where reaction rates at the crystal-melt interface are similar to the rates of diffusive transport of ions through the melt to the advancing crystal surface. To this end, we experimentally investigated euhedral plagioclase crystal shapes in dry mafic (basaltic) and hydrous silicic (haplodacitic) melts. Aspect ratios and inferred relative growth rates of the 3D short (S) and intermediate (I) crystal dimensions vary significantly between mafic and silicic melts, with $\delta S:\delta I = 1.6\text{--}1.20$ in basalt and $1.2.5\text{--}1.8$ in hydrous haplodacite. The lower aspect ratios of plagioclase grown in the silicic melt coincide with 10 to 100× lower melt diffusion rates than in the mafic melt. Using an anisotropic growth model, we show that such differences in melt diffusivity can explain the discrepancy in plagioclase aspect ratios: if interface reaction and melt diffusion rates are of similar magnitude, then the growth of a crystal facet with high interfacial reaction rates may be limited by melt diffusion, while another facet of the same crystal with lower interfacial reaction rates may grow uninhibited by melt diffusivity. This selective control of melt diffusion on crystal growth rates results in progressively more equant crystal shapes as diffusivity decreases, consistent with our experimental observations. Importantly, crystals formed in this diffusion-moderated, intermediate growth regime may not show any classical diffusion-controlled growth features. The proposed model was developed for plagioclase microlites but should be generalisable to all anisotropic microlite growth in volcanic rocks.

Keywords: crystal growth; crystal shape; interface kinetics; melt diffusivity; plagioclase

INTRODUCTION

Crystal growth rates and resulting crystal morphologies are controlled by two competing factors: (i) interface reaction kinetics, i.e. the rates at which atoms move across the melt-crystal interface; and (ii) diffusion in the melt, i.e. the rates of transport of atoms through the melt to the advancing crystal surface (e.g. reviews by Kirkpatrick, 1975 and Dowty, 1980). If the rates of interfacial reactions are much smaller than those of ion diffusion through the melt (e.g. at low melt supersaturation), then chemical supply at the crystal-melt interface is maintained and crystal growth rates are controlled by interface kinetics. In this interface-limited growth regime, relative growth rates of different crystal facets reflect variations in anisotropic crystal-melt interfacial energies, and the resulting crystal shapes are well-formed (euhedral; e.g. Kirkpatrick *et al.*, 1979; Muncill & Lasaga, 1987). On the other hand, if ion diffusion through the melt is slower than interfacial reaction rates (e.g. at high melt supersaturation), then compositional gradients develop in the melt and diffusion becomes the rate limiting process. Crystals formed in this diffusion-limited growth regime are typically skeletal, with acicular or bladed morphologies, or, in extreme cases, dendritic or spherulitic (e.g. Lofgren, 1974; Kirkpatrick *et al.*, 1979; Muncill & Lasaga, 1987;

Hammer & Rutherford, 2002; Duchêne *et al.*, 2008; Martel, 2012; Shea & Hammer, 2013). However, crystal growth under conditions where interfacial reaction rates and ion diffusivities in the melt are similar is less well understood. Here, we study plagioclase growth rates and resulting crystal morphologies in this intermediate growth regime of competing melt diffusivities and interfacial reaction rates. Firstly, we determine relative growth rates for the short and intermediate crystallographic axes of plagioclase in mafic and silicic melts through a series of novel crystallisation experiments. We then examine the relationship between relative crystal growth rates (and resulting plagioclase shapes) and melt diffusivities, and we present an anisotropic growth model predicting crystal shape as a function of competing interface reaction kinetics and melt diffusivities. We find that for an anisotropic crystal formed in the intermediate growth regime, some crystal faces may be affected by melt diffusion while others are not, resulting in variations in euhedral crystal shapes without necessarily producing typical diffusion-controlled textures.

EXPERIMENTAL APPROACH

To determine relative plagioclase growth rates in mafic and silicic melts, we conducted crystallisation experiments at low to

Received: January 24, 2023. Revised: June 29, 2023. Accepted: July 23, 2023

© The Author(s) 2023. Published by Oxford University Press.

This is an Open Access article distributed under the terms of the Creative Commons Attribution License (<http://creativecommons.org/licenses/by/4.0/>), which permits unrestricted reuse, distribution, and reproduction in any medium, provided the original work is properly cited.

moderate undercoolings ($\sim 0 < \Delta T < 70$ °C) designed to prevent diffusion-limited crystal growth. Absolute plagioclase growth rates derived from crystallisation experiments show relatively small variations (factor of 2–3) at such undercooling conditions for a given melt composition (Shea & Hammer, 2013). Assuming that relative growth rates along different growth directions (e.g. along the 3D short [S], intermediate [I] and long [L] growth direction) also remain approximately constant in this undercooling window, such relative plagioclase growth rates $\delta S:\delta I:\delta L$ can be constrained by characterising plagioclase shape as a function of crystal size. To this end, we ran a series of high-temperature crystallisation experiments producing a total range of 2D crystal lengths l from ~ 1 to 100 μm , with each experiment designed to produce one euhedral plagioclase population of a given size and shape. Crystal size was primarily controlled by inducing heterogeneous nucleation: at a given undercooling, crystals grow to smaller sizes as the number of nuclei increases (e.g. Martel, 2012; Mangler et al., 2022), hence, the higher the number of nucleation sites in an experiment, the smaller the resulting crystals. The number of available nucleation sites was adjusted by varying the particle size (i.e. surface area) of the starting glass: fine powder has a higher surface area than mm-sized chips of starting glass, and since each particle surface is a potential nucleation site (e.g. Zeng & Xu, 2015), starting glass powder generates a significantly higher nucleation density than chips when heated to (sub-) liquidus conditions. Additional controls used to modify final crystal size included varying (1) pre-experimental heating ramps and annealing steps, (2) experimental temperatures (i.e. undercooling), and (3) experimental durations (Table 1). An outline of specific experimental conditions is given below and in Table 1, and detailed experimental and analytical methods are provided in Supplementary File 1 and Tables S2 and S3.

For silicic compositions, we used a synthetic haplodacitic starting glass representative of melts in natural intermediate volcanic rocks (Table S1). Isothermal and single-step cooling experiments were conducted isobarically under H_2O -saturated conditions at 150 MPa and temperatures of 830 °C to 900 °C ($\sim 0 < \Delta T < 70$ °C) using a cold-seal pressure vessel at Durham University, UK (Table 1). The plagioclase liquidus under these conditions was experimentally determined to be at 890 ± 10 °C. Two series of crystallisation experiments were run: the first using finely powdered anhydrous starting glass to produce a high number of nuclei and hence small plagioclase crystal sizes (*High-N experiments*), and the second using chips of hydrated starting glass to produce lower numbers of larger plagioclase crystals (*Low-N experiments*; Table 1). In addition, pre-experimental heating ramps and dwells were used to promote varying degrees of nucleation (e.g. Corrigan, 1982; Lofgren, 1973; First et al., 2020), and experimental durations and temperatures were varied to probe different stages of growth (Table 1).

For mafic compositions, anhydrous crystallisation experiments were conducted at atmospheric pressure on a Linkam TS1500XY heating stage at Durham University using ≤ 60 μm thin, double-polished wafers of naturally glassy 'Blue Glassy Pahoehoe' basalt (Oze & Winter, 2005; Table S1). The plagioclase liquidus under experimental conditions was estimated to be $\sim 1180 \pm 5$ °C based on MELTS (Gualda & Ghiorso, 2015) and experimental observations (Geifman, 2022). Experiments were run at temperatures of 1180 °C to 1140 °C ($\sim 0 < \Delta T < 45$ °C; Table 1). Pre-experimental dwell times (1.5 to 10 minutes) and average cooling rates (0 to 4.3°C/min) were modulated to induce varying degrees of nucleation, and experiments were quenched after 3.5 to 142 minutes to capture different stages of plagioclase growth. Crystallisation

times were kept generally short to avoid overprinting of primary plagioclase shapes by oxide growth, crystal agglomeration (e.g. Pupier et al., 2008) or other maturation processes.

All experimental run products were sectioned, polished in γ - Al_2O_3 slurry and imaged on a Hitachi SU-70 field emission scanning electron microscope at Durham University. Crystal area as well as 2D lengths (l) and widths (w) were extracted manually using ImageJ (Schneider et al., 2012; Supplementary File 2). 3D crystal shapes for each sample were estimated from 2D l and w data using 2D-to-3D projection software *ShapeCalc* (Mangler et al., 2022). Since 3D crystal length (L) is poorly constrained by 2D intersection data (Higgins, 2000), the most significant morphological parameter is the ratio of 3D short/intermediate dimensions (S/I), and we, therefore, focus on relative growth rates $\delta S:\delta I$ and aspect ratios $S:I$ as a proxy for plagioclase shape in this study. Plagioclase size is expressed as the average crystal volume (Tables 1, S2, S3, Figs. 1 and 2), which is the inverse of the ratio of volumetric plagioclase number density $N_{v,plag}$ to plagioclase volume fraction ϕ_{plag} .

PLAGIOCLASE SHAPE EVOLUTION DURING GROWTH

The experiments produced plagioclase number densities of 10^3 to 10^7 mm^{-3} and average crystal lengths of 2 to 40 μm (Tables 1, S2, and S3), covering the range of microlite populations found in natural volcanic rocks (Cashman, 2020). Plagioclase crystal shapes are euhedral in all of our experiments, and textures indicative of diffusion-controlled growth are rare (Fig. 1). Crystal shapes in the haplodacite (blue in Fig. 1) vary from prismatic ($S/I=0.5$ or $S:I=1:2$) to tabular ($S/I=0.2$; $S:I=1:5$) with increasing size, consistent with observations in natural samples (Mangler et al., 2022). Contrary to previous experimental studies (e.g. Lofgren, 1974; Walker et al., 1976; Kirkpatrick et al., 1979; Shea & Hammer, 2013), we did not find a correlation between crystal shapes and nominal undercooling conditions (Fig. S1a), and there is also no clear correlation with plagioclase major element compositions (Fig. S1b; Supplementary Files 1 & 3). Plagioclase crystallised from basaltic melt (red in Fig. 1) shows an analogous trend from more prismatic ($S/I=0.26$; $S:I=1:4$) to more tabular shapes ($S/I=0.05$; $S:I=1:20$) with increasing size, but at generally lower S/I than in the haplodacite. This offset to lower S/I in the basaltic melt is consistent with our first-order petrographic observation that plagioclase generally forms thinner tablets in basalts than in rhyolites.

RELATIVE GROWTH RATES AND STEADY-STATE CRYSTAL SHAPES

Our knowledge about relative growth rates of different crystal facets in silicate minerals is limited. Mangler et al. (2022) showed that the change from prismatic to tabular plagioclase shapes with increasing microlite size can be reproduced by modelling crystal shape as a function of its growth volume, assuming a prismatic initial shape ($S/I=1$; $S:I=1:1$) and $10\times$ faster growth of the intermediate dimension than of the short dimension (i.e. relative growth rates $\delta S:\delta I=1:10$; $\delta S/\delta I=0.1$). These relative growth rates were determined by finding a fit to a complex natural dataset and are subject to large uncertainties. Here, we apply the same model to our more tightly controlled experimental size-shape data to infer robust constraints on relative growth rates along the short and intermediate crystallographic axes for plagioclase in basaltic and silicic melts (Fig. 2a & b). The growth model geometrically calculates the 3D shape change of a crystal with a given starting size and shape $S:I:L$ as it grows at given relative growth rates

Table 1: Experimental conditions and resulting plagioclase size and shape data

Experiment	Starting material	Heating ramp (h)*	Pre-experiment dwell	Initial T (°C)	Final T (°C)	Cooling rate (°C/min)	Run duration (h)	average V (μm ³)	S/#	± 1SD
Silicic experiments										
<i>High-N experiments</i>										
21-CSB-02	glass powder	1	-	900	900	isothermal	59	148	0.32	0.05
21-CSA-03	glass powder	0.67	-	900	900	isothermal	4	10	0.29	0.03
21-CSA-04	glass powder	0.92	-	900	900	isothermal	4	2	0.50	0.06
21-CSA-01_small	glass powder	1.75	-	900 (4 h)	830 (48 h)	single-step cooling	52	9	0.45	0.06
21-CSA-01_big	glass powder	1.75	-	900 (4 h)	830 (48 h)	single-step cooling	52	59	0.37	0.06
21-CSA-02	glass powder	1	-	900 (4 h)	830 (96 h)	single-step cooling	100	84	0.29	0.04
21-CSA-05	glass powder	0.83	-	900 (4 h)	830 (48 h)	single-step cooling	52	264	0.20	0.03
<i>Low-N experiments</i>										
22-CSA-01	glass chips	-	-	870	870	isothermal	78	754	0.20	0.03
22-CSB-03	glass chips	-	-	870	870	isothermal	168	7880	0.24	0.03
22-CSB-06	glass chips	-	-	870	870	isothermal	480	13 300	0.26	0.04
21-CSB-12_small	glass chips	-	-	850	850	isothermal	48	3	0.43	0.06
21-CSB-12_big	glass chips	-	-	850	850	isothermal	48	261	0.23	0.03
Basaltic experiments										
EG-BGP-2	glass wafer	0.1	170 s at 1180 °C	1180	1150	0.7	0.8	619	0.13	0.02
EG-BGP-3	glass wafer	0.1	600 s at 1180 °C	1180	1150	1.1	0.5	665	0.06	0.03
EG-BGP-4	glass wafer	0.1	140 s at 1180 °C	1180	1140	1.8	0.4	727	0.06	0.03
EG-BGP-5	glass wafer	0.1	300 s at 1180 °C	1180	1150	1.0	0.5	198	0.08	0.03
EG-BGP-6	glass wafer	0.1	90s at 1180 °C	1180	1155	0.2	2.4	345	0.08	0.03
EG-BGP-7	glass wafer	0.1	260 s at 1180 °C	1180	1150	0.4	1.1	169	0.16	0.03
HI-16-B-1	glass wafer	0.1	140 s at 1180 °C	1180	1165	4.3	0.1	20	0.23	0.04
HI-16-B-2	glass wafer	0.1	140 s at 1180 °C	1180	1180	isothermal	-	2	0.29	0.04

*Time to heat from room temperature to experimental run temperature #best estimate for 3D short over intermediate axis ± 1SD, calculated using ShapeCalc (Mangler et al., 2022).

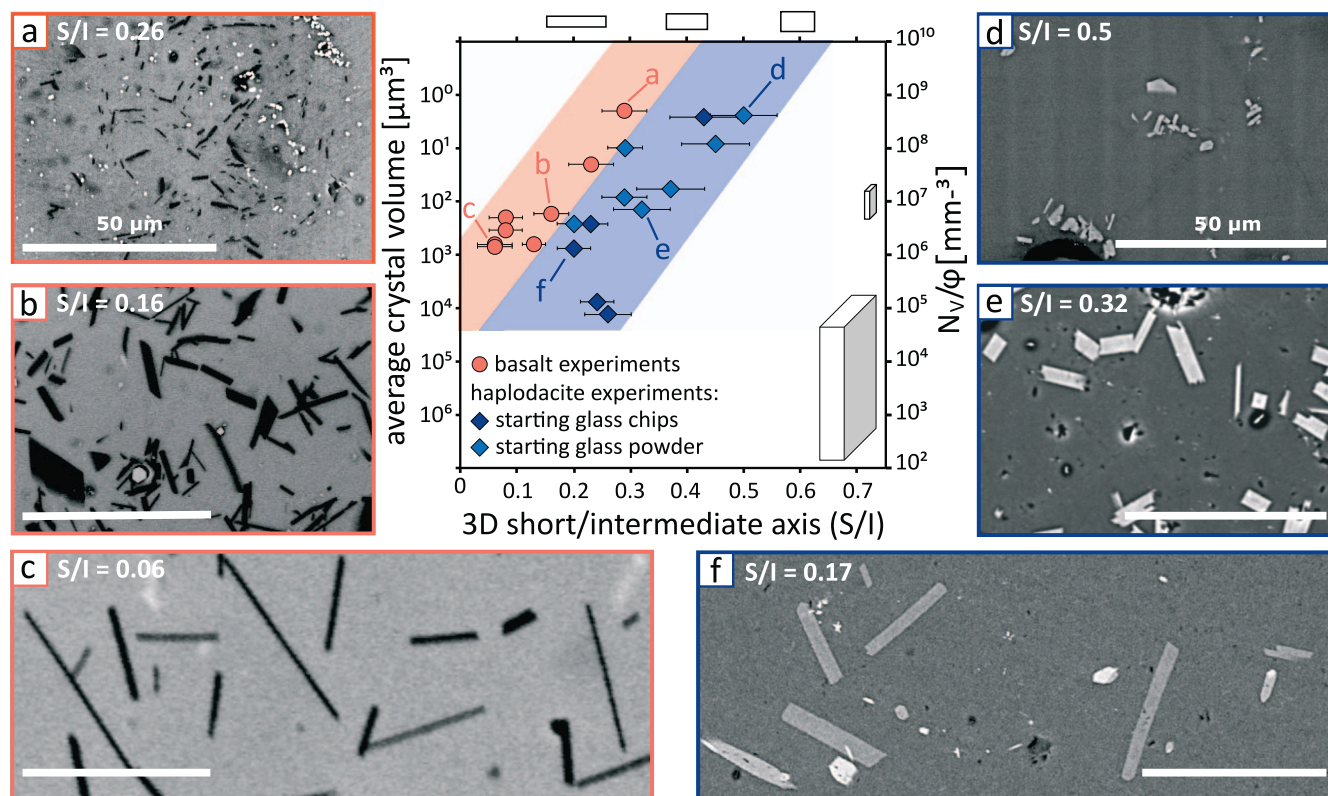


Fig. 1. Results of plagioclase crystallisation experiments. Crystal shape, expressed as the ratio of 3D short axis/intermediate axis ($S/I \pm 1SD$) becomes more tabular with increasing crystal volume, represented by the ratio of plagioclase number density N_V and crystallinity ϕ . Each datapoint reflects a single experiment, with the exception of 21-CSA-01 and 21-CSB-12, which are represented with two datapoints each to reflect their significant textural heterogeneity (Fig. S2). The range of plagioclase sizes and shapes is exemplified in (a)–(c) for basaltic experiments and in (d)–(f) for haplodacitic experiments. Note that plagioclase appears darker than the melt in basalt but slightly lighter in haplodacite due to the difference in melt compositions. Other minerals include Fe–Ti-oxides (bright crystals in (a) and (b)) and amphibole (bright crystals in (f)).

$\delta S:\delta l$ (Fig. S3). Following Mangler *et al.* (2022), we modelled crystal shape evolution for a ‘proto-crystal’ with an initial volume of $0.1 \mu\text{m}^3$, a prismatic starting shape ($S/I = 1$; $S:I = 1:1$), and relative growth rates $\delta S:\delta l$ of between 1:1.5 and 1:20 (Fig. 2a). The size-shape data for plagioclase crystallised from mafic melts show a good fit to models using relative growth rates $\delta S:\delta l$ of between 1:6 and 1:20 (shaded red in Fig. 2a & b). In contrast, best model fits for the haplodacite data suggests relative plagioclase growth rates of between 1:2.5 and 1:8 in the silicic melt (shaded blue in Fig. 2a & b).

The model results further show that crystal shapes rapidly approach aspect ratios defined by the relative growth rates after nucleation: once a crystal reaches a volume of $\sim 100 \mu\text{m}^3$ (corresponding to 2D crystal intersection lengths l of $> 5\text{--}15 \mu\text{m}$), its shape $S:I$ is predicted to become constant and reflect its relative growth rates $\delta S:\delta l$ (Fig. 2a & b). This is because the crystal volume added during growth is orders of magnitude larger than the proto-crystal volume, such that the initial shape is overprinted. Consistently, using a more tabular starting shape ($S/I = 0.75$; $S:I = 1:1.3$) does not significantly affect the fit of the model to our experimental data (Fig. 2b). Post-nucleation growth, therefore, leads to stable crystal shapes that reflect the relative growth rates along crystallographic axes ($S:I \approx \delta S:\delta l$), and we will refer to such crystal morphologies as *steady-state crystal shapes*. We suggest that euhedral microlites with volumes $> 100 \mu\text{m}^3$ generally exhibit such steady-state shapes, unless they are modified by a subsequent process (e.g. resorption and new growth with different $\delta S:\delta l$, or post-impingement growth). On the other hand, euhedral

crystals with volumes $< 100 \mu\text{m}^3$ ($l < 5\text{--}15 \mu\text{m}$) show transient morphologies tracing their evolution from proto-crystal to steady-state shapes.

MELT DIFFUSIVITY AFFECTS EUHEDRAL CRYSTAL GROWTH

Our experiments show that plagioclase morphology evolves during growth towards a steady-state crystal shape reflecting relative growth rates, which are different for mafic ($S/I \approx 0.05$; $S:I \approx 1:20$) and silicic melts ($S/I \approx 0.2$; $S:I \approx 1:5$). This difference in relative growth rates $\delta S:\delta l$ for plagioclase crystallised from mafic and silicic melts may reflect changes in the interfacial reaction rates of the short and intermediate growth directions. For example, temperature (Zanotto & James, 1985; Deubener & Weinberg, 1998; Hammer, 2008), relative crystal and melt compositions (Takei & Shimizu, 2003) and melt water content (Davis *et al.*, 1997; Hammer, 2004; Hammer, 2008; Mollard *et al.*, 2020) can all affect crystal-melt interfacial energies σ and may thus affect reaction rates. These parameters all have significantly different values for mafic and silicic systems and may, therefore, account for differences in total interfacial reaction rates. Importantly, such variations in σ would likely be anisotropic in nature, so they could explain differences in $\delta S:\delta l$ between mafic and silicic melts. However, interfacial energies of individual crystal faces of rock-forming minerals are unquantified except for olivine (Wanamaker & Kohlstedt, 1991; Watson *et al.*, 1997; Bruno *et al.*, 2014), precluding a quantitative assessment of the potential magnitude of these factors.

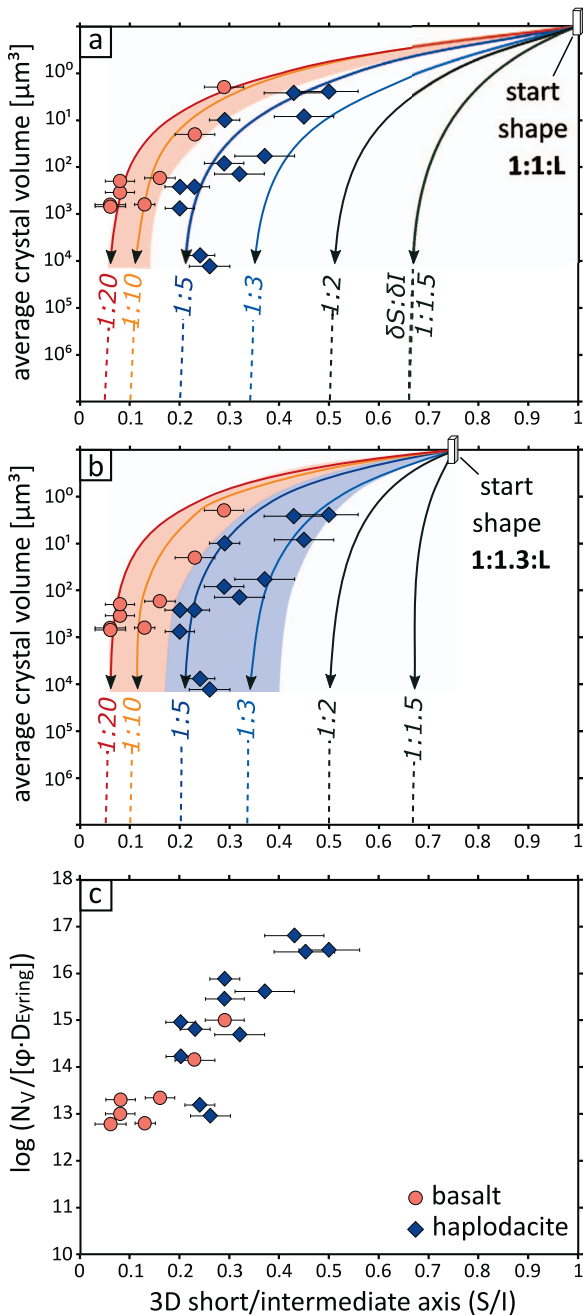


Fig. 2. (a) and (b) Models of crystal shape evolution with increasing volume for a range of growth rates $\delta S:\delta I$ for 3D relative short (S) and intermediate (I) dimensions ($\delta S:\delta I = 1:20$ – $1:1.5$). Starting point of the growth models is a crystal with a volume of $0.1 \mu\text{m}^3$ and a 3D start shape of (a) $S/I=1$ and (b) $S/I=0.75$. Relative growth rates for plagioclase grown from basaltic melt vary between $\delta S:\delta I = 1:6$ – $1:20$, whereas those for plagioclase crystallised from haplodacitic melt range from $\delta S:\delta I = 1:2.5$ – $1:8$. Note that shapes of crystals $>100 \mu\text{m}^3$ reflect relative growth rates ('steady-state crystal shapes'), and that variations of start shape do not significantly change outcomes. (c) The offset between the size-shape relationships of basaltic and haplodacitic experiments is removed by dividing the crystal volume factor $\frac{N_v}{\phi}$ by Eyring diffusivities of the melt. This suggests a kinetic control on euhedral crystal shapes. See text for discussion.

On the other hand, melt diffusivities are also strikingly different between the basalt and haplodacite. We used the Eyring equation to calculate the 'network diffusivity' at experimental conditions, which is analogous to the Si and O diffusivities in the

melts (Glasstone, 1941; Dingwell, 1990). Silicon and oxygen are the slowest diffusing elements of relevance and, therefore, limit chemical supply to the crystal-melt interface:

$$D_{\text{Eyring}} = \frac{k_B T}{\lambda \eta} \quad (1)$$

where k_B is the Boltzmann constant, T is the experimental temperature, λ is the diameter of the diffusing element (here set to 0.14 nm for O^{2-} ; Watkins et al., 2009), and η is the melt viscosity at experimental conditions calculated after Giordano et al. (2008). Eyring diffusivities are more than an order of magnitude lower in the hydrous haplodacite (between 4×10^{-15} and $1 \times 10^{-14} \text{ m}^2/\text{s}$) than in the basalt (between 2×10^{-13} and $5 \times 10^{-13} \text{ m}^2/\text{s}$; Tables S2 & S3). Such a large difference in melt diffusivity is likely to have an effect on crystal growth kinetics: the slower melt diffusion rates in the haplodacite could affect the melt composition at the advancing crystal-melt interface and, therefore, control absolute and relative growth rates. In fact, the two parallel size-shape trends for plagioclase crystallised from basalt and haplodacite (Fig. 1) collapse into a single correlation when normalised to the Eyring diffusivity for each experiment (Fig. 2c). This implies significant diffusion control on euhedral crystal growth. In other words, our experimental dataset offers a unique opportunity to study the *intermediate growth regime*, where diffusion competes with interfacial reaction as the rate-limiting process. In the following, we use a simple model to predict crystal shape as a function of melt diffusion and anisotropic interfacial reaction rates, and we examine our experimental data using the model.

INTERFACE REACTION V. DIFFUSION: A CRYSTAL GROWTH MODEL

In their work exploring effects of anisotropic Ostwald ripening in ceramics, Kitayama et al. (1998) introduced an equation to describe material flux across an interface i controlled by both diffusion in the melt and interfacial reaction:

$$J_i = -\frac{\Delta\mu_i}{k_b T V} \cdot \frac{DK_i}{D + K_i \Delta x} \quad (2)$$

where T is the temperature, V is the molar volume of the solid, D is the melt diffusion constant, Δx is the diffusion length, K_i is the interfacial reaction rate constant (c.f. Lai & Tien, 1993), and $\Delta\mu_i$ is the chemical potential difference between the melt phase and the crystal face i . Using the simplified assumption that $\Delta\mu_i$ is identical for all crystal-melt interfaces i (i.e. assuming that $\Delta\mu$ is not surface curvature dependent), we obtain a size-independent model describing relative growth rates of an anisotropic crystal as a function of diffusion and interface reaction rates:

$$\frac{\delta S}{\delta I} = \frac{K_S}{K_I} \cdot \frac{D + K_I \Delta x}{D + K_S \Delta x} \quad (3)$$

where $\delta S/\delta I$ describes the relative growth rates of the short (S) and intermediate (I) growth directions in terms of growth increments δS and δI . K_S and K_I are the interfacial reaction rate constants for S and I. A detailed derivation of and rationale for eq. (3) can be found in Supplementary File 1.

Firstly, we explore how the competition of melt diffusivity and interfacial reaction affects steady-state shapes using variable K_S , K_I , D and Δx in equation (3) (Fig. 3a & b). Following Kitayama et al. (1998), in order to directly compare melt diffusion

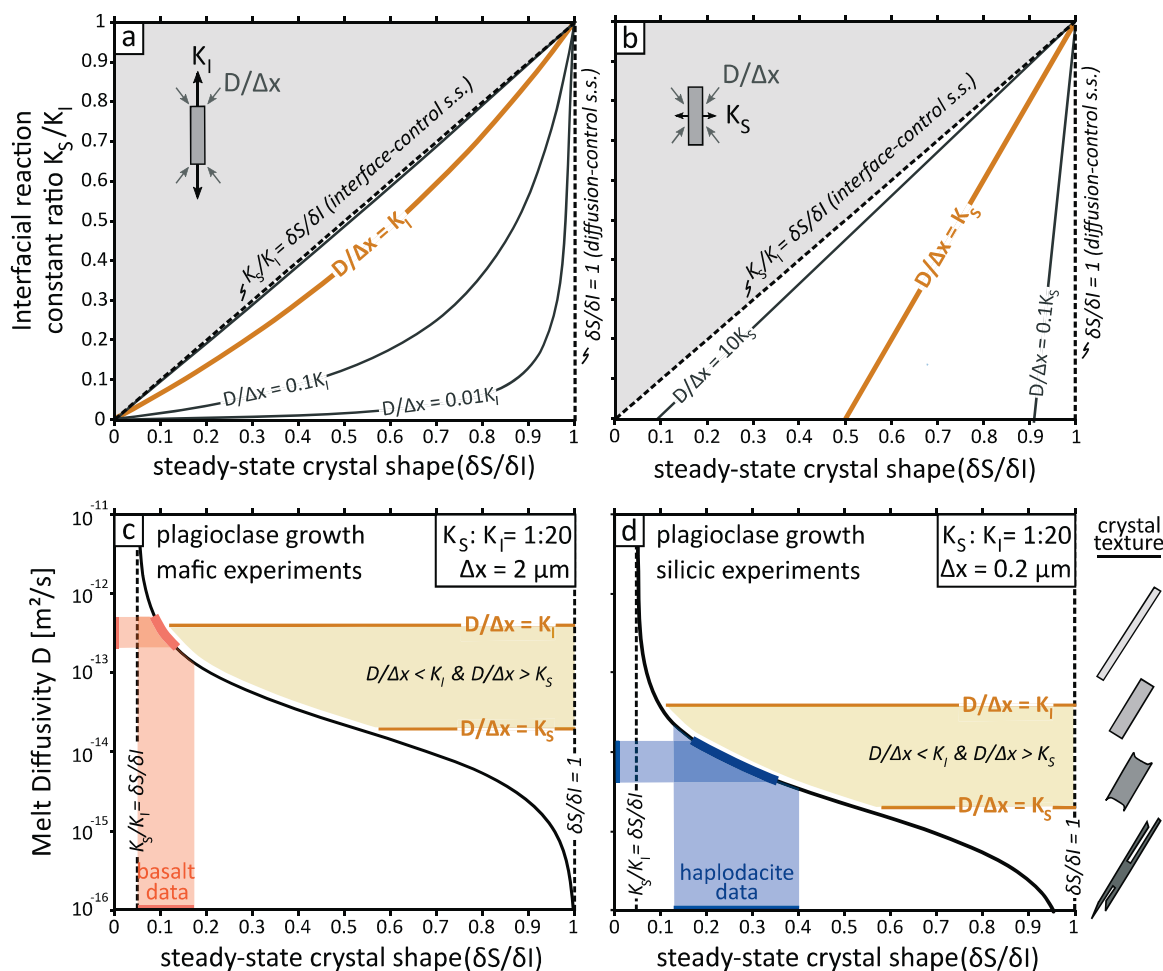


Fig. 3. Anisotropic growth modelling using equation (3). **(a)** and **(b)** Effect of melt diffusivities $D/\Delta x$ on resulting steady-state crystal shapes $\delta S/\delta l$ for a given interfacial reaction rate ratio K_S/K_I . **(a)** melt diffusivity relative to interface kinetics K_I of the intermediate growth dimension; **(b)** melt diffusivity relative to interface kinetics K_S of the short growth dimension. If diffusion is much faster than interfacial reaction ($D/\Delta x > 10K$), resulting steady-state crystal shapes approximate aspect ratios $\delta S/\delta l$ approaching K_S/K_I (dashed 1:1 line). Diffusion begins to affect crystal shapes even when $D/\Delta x > K$, and the point at which $D/\Delta x = K$ (orange curves) is reached earlier for the faster reacting intermediate growth direction than for the slower reacting short direction. Hence, growth of the intermediate crystal dimension is slowed down more significantly by melt diffusivity than growth of the short crystal dimension, resulting in increasing $\delta S/\delta l$ (i.e. lower aspect ratios) with decreasing diffusivity at a given K_S/K_I . Crystal shapes approach aspect ratios of 1 if melt diffusivity is much slower than interface kinetics ($D/\Delta x < 0.01K$), consistent with a completely diffusion-controlled growth regime (dashed vertical line). **(c)** and **(d)** Effect of varying melt diffusivity at fixed interfacial reaction constants $K_S:K_I=1:20$ ($K_S = 1 \cdot 10^{-8}$ m/s; $K_I = 2 \cdot 10^{-7}$ m/s) on steady-state crystal shape. Experimental melt diffusivities and steady-state plagioclase shapes are reproduced for **(a)** mafic experiments (red) at a diffusion length Δx of 2 μm and **(b)** silicic experiments (blue) at a diffusion length Δx of 0.2 μm . The yellow shaded area designates the intermediate growth regime in which melt diffusion is slower than interface kinetics of the intermediate growth direction but faster than interface kinetics of the slow growth direction. Resulting crystal morphologies with decreasing melt diffusivity are shown schematically to the right of panel d.

D [m^2/s] with interface reaction K_S and K_I [m/s], we examine the quantity $D/\Delta x$, which has units of [m/s]. It is clear from Fig. 3a & b that steady-state crystal shapes only show purely interface-controlled morphologies (i.e. $\delta S/\delta l = K_S/K_I$) if melt diffusion is at least $\sim 10\times$ faster than interfacial reaction ($D/\Delta x = 10K$). Significant deviations from purely interface-controlled morphologies are, therefore, possible even if melt diffusivities are higher than interface reaction rates. Crucially, the point at which diffusion rates and interfacial reaction rates are equal (i.e. $D/\Delta x = K$, yellow curve in Fig. 3a & b) is reached at higher melt diffusivity for growth of the intermediate dimension than for the short dimension, as K_I is larger than K_S . In other words, ion supply from the melt to the crystal-melt interface may slow down the advancement of fast growing crystal faces, whilst slower growing interfaces remain unaffected by melt diffusion. This qualitatively explains why lower melt diffusivities lead to crystals with lower aspect ratios (i.e. higher S/l). Finally, we point out that diffusion-

limited growth *sensu stricto* ($D/\Delta x \ll K$) would theoretically result in isotropic relative growth rates (i.e. $\delta S/\delta l = 1$, Fig. 3a & b). Strictly speaking, the *intermediate growth regime*, therefore, spans a large range (white area in Fig. 3a & b) and likely characterises most natural crystal growth. For practical use, we suggest a narrower definition of the intermediate growth regime as the case when melt diffusion is slower than interface reaction on some faces of a given crystal, but faster on other interfaces of the same crystal (e.g. $D/\Delta x < K_I$ but $D/\Delta x > K_S$, shown by the yellow area in Fig. 3c & d).

Next, we use equation (3) to examine how the competition between diffusion in the melt and interface kinetics might have shaped the steady-state crystal morphologies obtained in our mafic and silicic experiments (Fig. 3c & d). The interfacial reaction constants K_S and K_I depend on multiple parameters including the respective crystal-melt interfacial energies (Lai & Tien, 1993), which are unknown for plagioclase, and therefore, K_S and K_I cannot be independently constrained. Therefore, we used

representative experimental average plagioclase growth rates (c.f. Hammer, 2008) and set K_I to be 20 times higher than K_S ($K_S = 1 \times 10^{-8}$ m/s; $K_I = 2 \times 10^{-7}$ m/s), matching the maximum relative growth rates obtained in mafic experiments ($\delta S : \delta I = 1:20$, Fig. 2). Diffusivities D were varied between 10^{-11} and 10^{-16} m²/s to encompass Eyring diffusivities of our basaltic and haplodacitic experimental melts (Tables S2 & S3). The diffusion length can be expressed as $\Delta x = \sqrt{4Dt}$, and we used respective Eyring diffusivities and a diffusion time of $t = 1$ second to estimate diffusion lengths Δx of 2 μm for basaltic melts and 0.2 μm for silicic melts. Model results are shown in Fig. 3c and d for basaltic and silicic melts, respectively. Steady-state crystal shapes predicted for the respective experimental melt diffusivities are in good agreement with experimental steady-state plagioclase shapes for both mafic (shaded red in Fig. 3c) and silicic melts (shaded blue in Fig. 3d). The model, therefore, shows that the changes in plagioclase crystal shapes between mafic and silicic melts can be explained by variations in melt diffusivity alone, and variations in interfacial reaction rates are not required. We note, however, that K_S and K_I are likely to vary, as there is ample evidence that interfacial energies depend on curvature, temperature and composition (Davis et al., 1997; Deubener & Weinberg, 1998; Takei & Shimizu, 2003; Hammer, 2008; Schmelzer et al., 2019; Mollard et al., 2020). Nonetheless, based on our experimental data and model, we suggest that melt diffusivity plays a more important role in controlling euhedral crystal shapes than previously acknowledged. Lastly, we note that absolute plagioclase growth rates predicted by the model are about one to two orders of magnitude slower for silicic than for mafic melts, consistent with observations of lower plagioclase growth rates in rhyolitic than in andesitic experiments (Shea & Hammer, 2013). We, therefore, hypothesise that the well-documented differences in plagioclase growth rates for different melt compositions may be controlled by melt diffusivities.

Finally, we draw attention to the fact that in our experiments on both mafic and silicic melts, plagioclase appears to crystallise predominantly in the intermediate growth regime (i.e. $D/\Delta x < K_I$ but $D/\Delta x > K_S$, yellow area in Fig. 3c & d). This means that growth of the short crystal dimension S via interfacial reaction is slower than and unaffected by melt diffusion rates, whereas interface kinetics of the intermediate growth dimension I are faster than ion supply rates from the melt to the crystal-melt interface, and diffusion is thus limiting the intermediate growth rate. The result of this slowing down of δI relative to δS is a decrease in the aspect ratio of steady-state crystals, and it becomes more pronounced as melt diffusivity decreases (shown schematically in Fig. 3d). In addition, as D becomes increasingly rate limiting, Mullins-Sekerka instabilities (swallowtails) may begin to form on the faster growing interface (Fig. 3d), as commonly seen in natural volcanic rocks and occasionally in our experiments (Fig. 1e).

IMPLICATIONS FOR THE CRYSTALLISATION OF SILICATE MELTS

This study offers new insights into the crystallisation of silicate melts, with important implications for the interpretation of natural and experimental igneous rock textures.

1) There is no straightforward quantitative correlation between magma undercooling and crystal shape when nucleation is not exclusively homogeneous. Our experiments show that different crystal shapes (and sizes) form at identical undercoolings if the nucleation density is varied. Therefore, heterogeneous nucleation and pre-existing crystal cargo in natural magmas will also affect

crystal sizes and shapes, calling for extreme caution when using crystal textures to constrain undercooling conditions. This is particularly important at low undercoolings, for which heterogeneous nucleation is known to dominate (e.g. Fletcher, 1958; Chernov & Chernov, 1984; Liu, 2002).

2) Small microlites ($l < 5\text{--}15 \mu\text{m}$) show transient growth morphologies evolving from proto-crystal shapes towards aspect ratios reflecting the relative growth rates of their crystallographic axes. Larger euhedral crystals ($l > 5\text{--}15 \mu\text{m}$) exhibit steady-state crystal shapes, which reflect the relative growth rates that formed them.

3) Euhedral crystals may predominantly grow in an intermediate growth regime characterised by the competition between interface reaction rates and melt diffusivities, which control the rate of ion supply to the crystal-melt interface. Specifically, for anisotropic crystals, slower-growing crystal faces may grow uninhibited by melt diffusion kinetics, whereas faster-growing ones may already be limited by diffusion. This effect results in progressively lower aspect ratios as melt diffusivities decrease, and it can explain plagioclase shapes in natural magmas. In mafic melts, relatively high melt diffusivities will produce euhedral plagioclase morphologies approximating interfacial reaction rates. In more evolved silicate melts (e.g. dacite), melt diffusivities are lower and limit the growth rates of the fastest-growing crystal facets, thereby reducing the aspect ratios of steady-state shapes—without necessarily producing any of the classical diffusion-limited growth textures. Conversely, for a given melt diffusivity, higher absolute interface reaction rates (even if the ratio K_S/K_I remains constant) will result in an earlier onset of diffusion-moderated growth and, therefore, lower aspect ratio (higher S/I) crystals. The general model proposed here of diffusion-moderated crystal growth in an intermediate growth regime likely also applies to other anisotropic mineral phases (e.g. clinopyroxene and olivine).

4) Relative growth rates for plagioclase presented here describe post-nucleation growth outside the diffusion-controlled regime. The resulting steady-state crystal shapes are the first iteration of a crystal's morphology during its lifetime: our experiments chart plagioclase shape evolution during the initial two hours for basaltic melts (142 minutes, Table 1), and three weeks for silicic melts. Upon longer storage and textural maturation in magmatic systems, further modifications to crystal shapes are to be expected, such as heterogeneous nucleation on existing grains, post-impingement growth (Holness, 2014), crystal agglomeration (Pupier et al., 2008), or resorption. Hence, in order to better understand crystal shape and its petrological significance in volcanic rocks, more work is required to constrain textural maturation mechanisms and their timescales.

FUNDING

This work was funded by UK Natural Environment Research Council grant NE/T000430/1. This project has received funding from the European Research Council (ERC) under the European Union's Horizon 2020 research and innovation programme (grant agreement 864923). MCSH acknowledges support from a Royal Society research grant, RG120246. AAI acknowledges support from The Leverhulme Trust through an Early Career Fellowship.

DATA AVAILABILITY

The data underlying this article are available in its online supplementary material.

SUPPLEMENTARY DATA

Supplementary data are available at *Journal of Petrology* online.

ACKNOWLEDGMENTS

We thank Jenni Barclay for donating her cold-seal pressure vessel setup and Leon Bowen of the GJ Russell Electron Microscopy Facility at Durham University for facilitating SEM analysis. We are grateful to Ed Llewellyn for providing the blue glassy pahoehoe sample material that is used in Geifman (2022), and which is analysed herein. We thank the editor Takashi Mikouchi, as well as Silvio Mollo, Akira Tsuchiyama and Monika Rusiecka for insightful reviews which helped improve the manuscript.

References

- Bruno, M., Massaro, F. R., Prencipe, M., Demichelis, R., De La Pierre, M. & Nestola, F. (2014). Ab initio calculations of the main crystal surfaces of forsterite (Mg₂SiO₄): a preliminary study to understand the nature of geochemical processes at the olivine interface. *The Journal of Physical Chemistry C* **118**(5), 2498–2506. <https://doi.org/10.1021/jp409837d>.
- Cashman, K. V. (2020). Crystal size distribution (CSD) analysis of volcanic samples: advances and challenges. *Frontiers in Earth Science* **8**, 1–17. <https://doi.org/10.3389/feart.2020.00291>.
- Chernov, A. A. & Chernov, A. A. (1984). *Modern Crystallography III: Crystal Growth*, pp.48–103.
- Corrigan, G. M. (1982). Supercooling and the crystallization of plagioclase, olivine, and clinopyroxene from basaltic magmas. *Mineralogical Magazine* **46**(338), 31–42. <https://doi.org/10.1180/minmag.1982.046.338.06>.
- Davis, M. J., Ihinger, P. D. & Lasaga, A. C. (1997). Influence of water on nucleation kinetics in silicate melt. *Journal of Non-Crystalline Solids* **219**, 62–69. [https://doi.org/10.1016/S0022-3093\(97\)00252-4](https://doi.org/10.1016/S0022-3093(97)00252-4).
- Deubener, J. & Weinberg, M. C. (1998). Crystal–liquid surface energies from transient nucleation. *Journal of Non-Crystalline Solids* **231**(1–2), 143–151. [https://doi.org/10.1016/S0022-3093\(98\)00412-8](https://doi.org/10.1016/S0022-3093(98)00412-8).
- Dingwell, D. B. (1990). Effects of structural relaxation on cationic tracer diffusion in silicate melts. *Chemical Geology* **82**, 209–216. [https://doi.org/10.1016/0009-2541\(90\)90082-1](https://doi.org/10.1016/0009-2541(90)90082-1).
- Dowty, E. (1980). Crystal growth and nucleation theory and the numerical simulation of igneous crystallization. In: *Physics of magmatic processes*. Princeton University Press, pp.419–486.
- Duchêne, S., Pupier, E., De Veslud, C. L. C. & Toplis, M. J. (2008). A 3D reconstruction of plagioclase crystals in a synthetic basalt. *American Mineralogist* **93**(5–6), 893–901. <https://doi.org/10.2138/am.2008.2679>.
- First, E. C., Leonhardi, T. C. & Hammer, J. E. (2020). Effects of superheating magnitude on olivine growth. *Contributions to Mineralogy and Petrology* **175**, 1–14. <https://doi.org/10.1007/s00410-019-1638-7>.
- Fletcher, N. H. (1958). Size effect in heterogeneous nucleation. *The Journal of Chemical Physics* **29**(3), 572–576. <https://doi.org/10.1063/1.1744540>.
- Geifman, E. (2022) *Determining the Effects of Cooling Rate on Magma Crystallisation Using a High Temperature Heating Stage* MSc thesis. Durham University.
- Giordano, D., Russell, J. K. & Dingwell, D. B. (2008). Viscosity of magmatic liquids: a model. *Earth and Planetary Science Letters* **271**(1–4), 123–134. <https://doi.org/10.1016/j.epsl.2008.03.038>.
- Glasstone, S. (1941). Viscosity and diffusion. *The Theory of Rate Processes* **477**.
- Gualda, G. A. R. & Ghiorso, M. S. (2015). MELTS_excel: A Microsoft Excel-based MELTS interface for research and teaching of magma properties and evolution. *Geochemistry, Geophysics, Geosystems* **16**(1), 315–324. <https://doi.org/10.1002/2014GC005545>.
- Hammer, J. E. (2004). Crystal nucleation in hydrous rhyolite: experimental data applied to classical theory. *American Mineralogist* **89**(11–12), 1673–1679. <https://doi.org/10.2138/am-2004-11-1212>.
- Hammer, J. E. (2008). Experimental studies of the kinetics and energetics of magma crystallization. *Reviews in Mineralogy and Geochemistry* **69**(1), 9–59. <https://doi.org/10.2138/rmg.2008.69.2>.
- Hammer, J. E. & Rutherford, M. J. (2002). An experimental study of the kinetics of decompression-induced crystallization in silicic melt. *Journal of Geophysical Research: Solid Earth* **107**(B1), ECV 8-1–ECV 8-24. <https://doi.org/10.1029/2001jb000281>.
- Higgins, M. D. (2000). Measurement of crystal size distributions. *American Mineralogist* **85**(9), 1105–1116. <https://doi.org/10.2138/am-2000-8-901>.
- Holness, M. B. (2014). The effect of crystallization time on plagioclase grain shape in dolerites. *Contributions to Mineralogy and Petrology* **168**(5). <https://doi.org/10.1007/s00410-014-1076-5>.
- Kirkpatrick, R. J. (1975). Crystal growth from the melt: a review. *American Mineralogist: Journal of Earth and Planetary Materials* **60**(9–10), 798–814.
- Kirkpatrick, R. J., Klein, L., Uhlmann, D. R. & Hays, J. F. (1979). Rates and processes of crystal growth in the system anorthite-albite. *Journal of Geophysical Research: Solid Earth* **84**(B7), 3671–3676. <https://doi.org/10.1029/JB084iB07p03671>.
- Kitayama, M., Hira, O. K., Toriyama, M. & Kanzaki, S. (1998). Modeling and simulation of grain growth in Si₃N₄—I. anisotropic Ostwald ripening. *Acta Materialia* **46**(18), 6541–6550. [https://doi.org/10.1016/S1359-6454\(98\)00290-0](https://doi.org/10.1016/S1359-6454(98)00290-0).
- Lai, K. R. & Tien, T. Y. (1993). Kinetics of β -Si₃N₄ grain growth in Si₃N₄ ceramics sintered under high nitrogen pressure. *Journal of the American Ceramic Society* **76**(1), 91–96. <https://doi.org/10.1111/j.1151-2916.1993.tb03693.x>.
- Liu, X. Y. (2002). Effect of foreign particles: a comprehensive understanding of 3D heterogeneous nucleation. *Journal of Crystal Growth* **237–239**, 1806–1812. [https://doi.org/10.1016/S0022-0248\(01\)02348-X](https://doi.org/10.1016/S0022-0248(01)02348-X).
- Lofgren, G. (1973). Effect of heterogeneous nucleation on basaltic textures: a dynamic crystallization study. *Journal of Petrology* **24**(3), 229–255. <https://doi.org/10.1093/petrology/24.3.229>.
- Lofgren, G. (1974). An experimental study of plagioclase crystal morphology; isothermal crystallization. *American Journal of Science* **274**(3), 243–273. <https://doi.org/10.2475/ajs.274.3.243>.
- Mangler, M. F., Humphreys, M. C. S., Wadsworth, F. B., Iveson, A. A. & Higgins, M. D. (2022). Variation of plagioclase shape with size in intermediate magmas: a window into incipient plagioclase crystallisation. *Contributions to Mineralogy and Petrology* **177**, 64. <https://doi.org/10.1007/s00410-022-01922-9>.
- Martel, C. (2012). Eruption dynamics inferred from microlite crystallization experiments: application to Plinian and dome-forming eruptions of Mt. Pelée (Martinique, Lesser Antilles). *Journal of Petrology* **53**(4), 699–725. <https://doi.org/10.1093/petrology/egr076>.
- Mollard, E., Martel, C., Le Trong, E. & Rogerie, G. (2020). Theoretical models of decompression-induced plagioclase nucleation and growth in hydrated silica-rich melts. *Frontiers in Earth Science* **8**, 203. <https://doi.org/10.3389/feart.2020.00203>.
- Muncill, G. E. & Lasaga, A. C. (1987). Crystal-growth kinetics of plagioclase in igneous systems; one-atmosphere experiments and application of a simplified growth model. *American Mineralogist* **72**(3–4), 299–311.

- Oze, C. & Winter, J. D. (2005). The occurrence, vesiculation, and solidification of dense blue glassy pahoehoe. *Journal of Volcanology and Geothermal Research* **142**(3–4), 285–301. <https://doi.org/10.1016/j.jvolgeores.2004.11.008>.
- Pupier, E., Duchene, S. & Toplis, M. J. (2008). Experimental quantification of plagioclase crystal size distribution during cooling of a basaltic liquid. *Contributions to Mineralogy and Petrology* **155**(5), 555–570. <https://doi.org/10.1007/s00410-007-0258-9>.
- Schmelzer, J. W., Abyzov, A. S., Ferreira, E. B. & Fokin, V. M. (2019). Curvature dependence of the surface tension and crystal nucleation in liquids. *International Journal of Applied Glass Science* **10**(1), 57–68. <https://doi.org/10.1111/ijag.12900>.
- Schneider, C. A., Rasband, W. S. & Eliceiri, K. W. (2012). NIH image to ImageJ: 25 years of image analysis. *Nature Methods* **9**(7), 671–675. <https://doi.org/10.1038/nmeth.2089>.
- Shea, T. & Hammer, J. E. (2013). Kinetics of cooling- and decompression-induced crystallization in hydrous mafic-intermediate magmas. *Journal of Volcanology and Geothermal Research* **260**, 127–145. <https://doi.org/10.1016/j.jvolgeores.2013.04.018>.
- Takei, Y. & Shimizu, I. (2003). The effects of liquid composition, temperature, and pressure on the equilibrium dihedral angles of binary solid–liquid systems inferred from a lattice-like model. *Physics of the Earth and Planetary Interiors* **139**(3–4), 225–242. <https://doi.org/10.1016/j.pepi.2003.08.004>.
- Walker, D., Kirkpatrick, R. J., Longhi, J. & Hays, J. F. (1976). Crystallization history of lunar picritic basalt sample 12002: phase-equilibria and cooling-rate studies. *Geological Society of America Bulletin* **87**(5), 646. [https://doi.org/10.1130/0016-7606\(1976\)87<646:Cholpb>2.0.Co;2](https://doi.org/10.1130/0016-7606(1976)87<646:Cholpb>2.0.Co;2).
- Wanamaker, B. J. & Kohlstedt, D. L. (1991). The effect of melt composition on the wetting angle between silicate melts and olivine. *Physics and Chemistry of Minerals* **18**(1), 26–36. <https://doi.org/10.1007/BF00199040>.
- Watkins, J. M., DePaolo, D. J., Huber, C. & Ryerson, F. J. (2009). Liquid composition-dependence of calcium isotope fractionation during diffusion in molten silicates. *Geochimica et Cosmochimica Acta* **73**(24), 7341–7359. <https://doi.org/10.1016/j.gca.2009.09.004>.
- Watson, G. W., Oliver, P. M. & Parker, S. C. (1997). Computer simulation of the structure and stability of forsterite surfaces. *Physics and Chemistry of Minerals* **25**, 70–78. <https://doi.org/10.1007/s002690050088>.
- Zanotto, E. D. & James, P. F. (1985). Experimental tests of the classical nucleation theory for glasses. *Journal of Non-Crystalline Solids* **74**(2–3), 373–394. [https://doi.org/10.1016/0022-3093\(85\)90080-8](https://doi.org/10.1016/0022-3093(85)90080-8).
- Zeng, Q. & Xu, S. (2015). Thermodynamics and characteristics of heterogeneous nucleation on fractal surfaces. *The Journal of Physical Chemistry C* **119**(49), 27426–27433. <https://doi.org/10.1021/acs.jpcc.5b07709>.